Cell, Vol. 111, 129–140, October 4, 2002, Copyright ©2002 by Cell Press

Orientation of Ribosome Recycling Factor in the Ribosome from Directed Hydroxyl Radical Probing

Laura Lancaster,[1] Michael C. Kiel,[2] Akira Kaji,[2] and Harry F. Noller[1,3]

[1]Center for Molecular Biology of RNA
Sinsheimer Laboratories
University of California, Santa Cruz
Santa Cruz, California 95064

[2]Department of Microbiology
School of Medicine
University of Pennsylvania
Philadelphia, Pennsylvania 19104

Summary

Ribosome recycling factor (RRF) disassembles posttermination complexes in conjunction with elongation factor EF-G, liberating ribosomes for further rounds of translation. The striking resemblance of its L-shaped structure to that of tRNA has suggested that the mode of action of RRF may be based on mimicry of tRNA. Directed hydroxyl radical probing of 16S and 23S rRNA from Fe(II) tethered to ten positions on the surface of *E. coli* RRF constrains it to a well-defined location in the subunit interface cavity. Surprisingly, the orientation of RRF in the ribosome differs markedly from any of those previously observed for tRNA, suggesting that structural mimicry does not necessarily reflect functional mimicry.

Introduction

Ribosome recycling is a required step in protein synthesis that occurs after termination and, in bacteria, is catalyzed by the ribosome recycling factor (RRF) (for reviews, see Janosi et al., 1996a, 1996b; Kaji and Hirokawa, 2000; Kaji et al., 2001), an essential protein (Janosi et al., 1994). After reaching the end of a protein-coding sequence, the ribosome binds release factor RF-1 or RF-2 in response to a stop codon in the ribosomal A site, activating hydrolysis of the polypeptide chain from peptidyl-tRNA (for a review, see Poole and Tate, 2000). Release factor RF-3 then catalyzes dissociation of RF-1 or RF-2 (Freistroffer et al., 1997), leaving a posttermination complex consisting of the 70S ribosome, mRNA, and deacylated tRNA in the P site. RRF works in concert with elongation factor G (EF-G) and GTP to disassemble the posttermination complex, freeing the ribosome for the next round of translation (Hirashima and Kaji, 1970, 1972, 1973; Ogawa and Kaji, 1975).

While the mechanism for disassembly is not well understood, several studies have provided insight into the function of RRF. In the classical in vitro experiments, posttermination complexes formed either from naturally occurring polysomes or constructed with a phage RNA are disassembled by RRF and EF-G into free ribosomes, mRNA, and deacylated tRNA (Hirashima and Kaji, 1972; Ogawa and Kaji, 1975; Hirokawa et al., 2002b). In studies performed using a short synthetic mRNA containing a strong Shine-Dalgarno sequence, RRF and EF-G separate the ribosomal subunits, leaving a 30S subunit-mRNA-tRNA complex (Karimi et al., 1999). The bound tRNA is in turn released from the complex by initiation factor IF-3. Recent in vivo evidence suggests that the context of mRNA near the termination site influences whether or not ribosomes are completely dissociated from mRNA by RRF and EF-G during recycling (Inokuchi et al., 2000). It has been inferred that RRF binds to the ribosomal A site because it competes for binding to ribosomes with RF-1 (Pavlov et al., 1997), which is believed to bind the A site. RRF also inhibits binding of N-acetyl-phenylalanyl-tRNA to nonprogrammed ribosomes, suggesting an interaction of RRF with the P site (Hirokawa et al., 2002a). In the absence of RRF, ribosomes remain bound to mRNA after termination of protein synthesis and reinitiate unscheduled translation downstream of the mRNA stop codon both in vitro (Ryoji et al., 1981) and in vivo (Janosi et al., 1998). Genetic evidence for a functional interaction between RRF and EF-G has been shown by rescue of an *Escherichia coli* temperature-sensitive RRF strain by simultaneous expression of RRF and EF-G from *Mycobacterium tuberculosis*, whereas expression of either factor alone failed to rescue the strain (Rao and Varshney, 2001). Potential contact sites between RRF and EF-G have been identified by a genetic mutation and selection study (Ito et al., 2002).

The RRF structure, which has been solved for four different organisms (Selmer et al., 1999; Kim et al., 2000; Toyoda et al., 2000; Yoshida et al., 2001), is comprised of a 3 helix bundle (domain I) connected to a smaller, α/β domain (domain II). The four RRF structures are very similar except for the orientation of the two domains with respect to one another (Figure 1A). The RRF structure strongly resembles that of tRNA, prompting Selmer et al. (1999) to propose that RRF binds to the vacant A site of the posttermination complex and is then translocated like a tRNA to the P site by EF-G, resulting in ejection of the deacylated tRNA and disassembly of the complex.

In this study, we used directed hydroxyl radical probing of rRNA from Fe(II)-derivatized RRF proteins bound to 70S ribosomes to generate constraints for modeling the position and orientation of RRF in the 5.5 Å crystal structure of the complete ribosome (Yusupov et al., 2001). Unexpectedly, our data indicate that RRF binds to the ribosome in an orientation that differs markedly from that of tRNA, suggesting that its mode of action is not based on straightforward mimicry of tRNA.

Results

Construction, Purification, and Activity of Mutant RRF Proteins

We used site-directed mutagenesis to construct single-cysteine mutations in the *E. coli* RRF protein for attaching Fe(II)-BABE probes. First, the naturally-occurring cysteine at position 16 was replaced with serine to

[3]Correspondence: harry@nuvolari.ucsc.edu

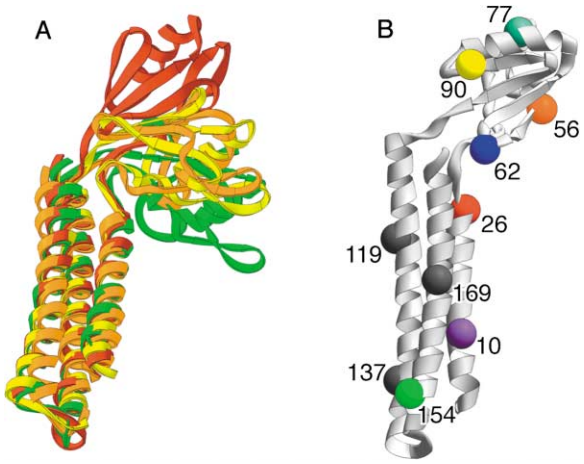

Figure 1. Positions of Single-Cysteine Mutations in RRF and Comparison of Four RRF Structures

(A) Superposition of domain I of RRF structures from *T. maritima* (Selmer et al., 1999) (green), *T. thermophilus* (Toyoda et al., 2000) (yellow), *A. aeolicus* (Yoshida et al., 2001) (orange), and *E. coli* (Kim et al., 2000) (red).

(B) The crystal structure of *E. coli* RRF (Kim et al., 2000) in light gray shown with the locations of single cysteines introduced as probe-attachment sites at positions 10 (purple), 26 (red), 56 (orange), 62 (blue), 77 (turquoise), 90 (yellow), 119 (gray), 137 (gray), 154 (green), and 169 (gray). Cleavage of rRNA was not observed from positions 119, 137, and 169.

give a cysteine-free version of RRF, RRF(-cys), whose biological activity was confirmed by its ability to rescue both a strain containing a temperature-sensitive RRF allele and a strain lacking a functional RRF allele (data not shown). RRF(-cys) then served as a starting construct for introducing single-cysteine mutations at ten well-distributed, surface-accessible, phylogenetically variable residues (Figure 1B). The mutant RRF proteins were overexpressed, purified by cation and anion exchange FPLC, and derivatized with Fe(II)-BABE for probing or with [^{14}C]iodoacetamide for binding studies.

We tested the binding of mutant RRF proteins to ribosomes by forming complexes of the ^{14}C-labeled RRF mutants with 30S subunits, 50S subunits, or 70S ribosomes, using a 10-fold molar excess of RRF protein over ribosomal particle. Free RRF was removed by centrifugation through Microcon 100 filters, and the bound protein was detected by scintillation counting. All of the derivatized RRF mutants bound 70S ribosomes (Table 1). Several of the labeled mutant RRF proteins were tested for binding to 30S and 50S subunits; all bound to 50S subunits, but showed little or no interaction with 30S subunits.

Fe(II)-BABE modified RRF mutant proteins were tested for their activity in converting polysomes to monosomes using approximately an equimolar equivalent of RRF per ribosome equivalent. All of the Fe(II)-RRF proteins tested showed activity in the range of 44%–117% compared to wild-type RRF (Table 1).

Probing the rRNA Region Surrounding RRF

Complexes were formed containing either mock derivatized RRF(-cys) or Fe(II)-BABE-RRF bound to 70S *E. coli* ribosomes, or to 70S ribosome complexes containing mRNA and deacylated tRNA, similar to the natural substrate of RRF. Cleavage of the 23S rRNA and 16S rRNA backbones by hydroxyl radicals generated from the tethered Fe(II) was detected by primer extension (Figure 2) and scored as described in Experimental Procedures. Unique cleavage patterns were obtained from seven of the ten probing positions, as summarized in Figure 3. Fe(II)-RRF cleaved 23S rRNA in the P-tRNA and A-tRNA binding regions, sarcin loop, and L11 binding region, and cleaved 16S rRNA near the top of the penultimate stem.

Position 154, near the tip of RRF domain I (Figure 1B), cleaved nucleotides in 23S rRNA helix 74 (2063-2064) and helix 93 (2593-2594 and 2601-2603), which flank the P-tRNA side of the peptidyl transferase region (Figures 2D, 2G, and 3). Position 10, also in domain I, extensively cleaved the 23S rRNA A-tRNA binding region, including

Table 1. Binding of [^{14}C]-Acetamido-RRF Mutant Proteins to Ribosomes and Activity of Fe(II)-RRF Mutant Proteins in Conversion of Polysomes to Monosomes

	Ribosome Binding[a]			Polysome Conversion Assay[b]	
RRF Probe Position	70S	30S	50S	% Conversion	Relative Activity[c]
10	0.96 ± 0.03	0	0.68 ± 0.1	40	1.04
26	1.0 ± 0.3	0.2	0.76 ± 0.2	n.d.	n.d.
56	1.0 ± 0.1	0	0.68 ± 0.1	20	0.52
62	1.0 ± 0.3	0	0.60 ± 0.0	17	0.44
77	1.3 ± 0.0	0.2	1.0 ± 0.1	20	0.52
90	0.77 ± 0.03	n.d.	n.d.	45	1.17
119	0.97 ± 0.03	n.d.	n.d.	24	0.62
137	1.0 ± 0.1	n.d.	n.d.	n.d.	n.d.
154	0.83 ± 0.3	n.d.	n.d.	17	0.44
169	0.77 ± 0.2	n.d.	n.d.	23	0.60

Abbreviation: n.d., not determined.

[a] Values are reported as pmol of RRF bound per pmol of ribosomal particle added (see Experimental Procedures), using a 10-fold molar excess of RRF over ribosomes. Data are the average of three independent measurements for 70S, two measurements for 50S, and a single measurement for 30S.

[b] Values are reported as the activity of mutant Fe(II)-RRF proteins in converting polysomes to monosomes (see Experimental Procedures), using an approximate equimolar equivalent of RRF per ribosome equivalent.

[c] Activity relative to that of wild-type RRF, set to 1.0.

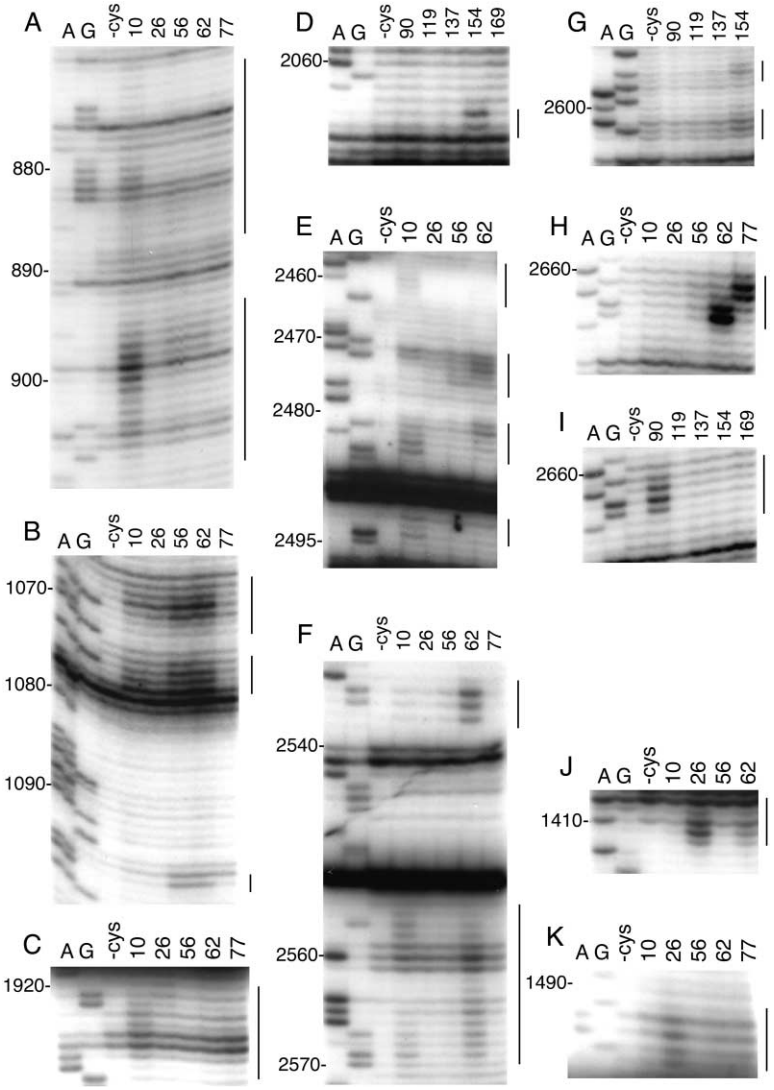

Figure 2. Directed Hydroxyl Radical Probing of 16S and 23S rRNA from Fe(II)-RRF-70S Ribosome Complexes Detected by Primer Extension

(A–I) 23S rRNA

(J–K) 16S rRNA

The letters A and G indicate sequencing lanes. All other lanes are from 70S ribosomes probed with bound mock-derivatized RRF(-cys), or with mutant versions of RRF derivatized by Fe(II)-BABE at positions 10, 26, 56, 62, 77, 90, 119, 137, 154, or 169.

helix 89 (2459-2462, 2470-2471, 2479-2483, and 2491-2493), helix 90 (2565-2570), helix 92 (2555-2557), and the A site finger helix 38 (878-882 and 894-906) (Figures 2E, 2F, 2A, and 3). 23S rRNA helix 69 (1921-1926 and 1908-1910), near the P-tRNA, and helix 43 (1065-1068 and 1073-1075), part of the L11 binding region, are weakly cleaved from position 10 (Figures 2C, 2B, and 3). Position 26, at the end of domain I near the hinge, cleaved the 16S rRNA penultimate stem (helix 44, nucleotides 1408-1411 and 1492-1494) and weakly cleaved 23S rRNA helix 69 (1919-1921) and helix 43 (1065-1068) (Figures 2J, 2K, 2C, 2B, and 3). Position 62, in domain II and also near the hinge, cleaved nucleotides in 23S rRNA helix 89 (2470-2474 and 2479-2480) and helix 92 (2555-2568), which are close to the A-tRNA, helix 91 (2534-2536), between the A-tRNA and sarcin loop, the sarcin loop (helix 95, nucleotides 2662-2663), and helices 43 (1065-1068 and 1072-1075) and 44 (1094-1095) in the LII binding region (Figures 2E, 2F, 2H, 2B, and 3). Position 62 weakly cleaved 16S rRNA helix 44 (1408-1411) (Figures 2J and 3). The 23S rRNA sarcin loop (helix 95) was also cleaved from domain II positions 77 (nucleotides 2659-2661) and 90 (2660-2663) (Figures 2H, 2I, and 3). Position 56, in domain II, cleaved the L11 binding region helices 43 (1065-1068 and 1072-1075) and 44 (1094-1095) and weakly cleaved 23S rRNA helix 89 (2470-2474) (Figures 2B, 2E, and 3). We failed to observe cleavage of rRNA from positions 119, 137, or 169, all located in domain I.

Complexes of 70S ribosomes containing poly(U) mRNA and N-acetyl-[^{14}C]-Phe-tRNA were made. Binding to the ribosomal P site was confirmed by filter binding (93%–96%), puromycin reactivity (88%–90%), and footprinting on rRNA (Figure 4A). Reaction of the complex with puromycin resulted in the characteristic enhanced reactivity of A702 of 16S rRNA toward dimethyl sulfate (Figure 4A; Moazed and Noller, 1989a), while maintaining the 16S rRNA P site footprint. This result confirmed the conversion of N-Acetyl-Phe-tRNA to its deacylated form, and movement of the tRNA from the P/P into the P/E hybrid state, as expected. Similar footprints were observed after addition of a 10-fold molar excess of RRF over ribosomes under the same conditions used for the probing experiments (Figure 4A).

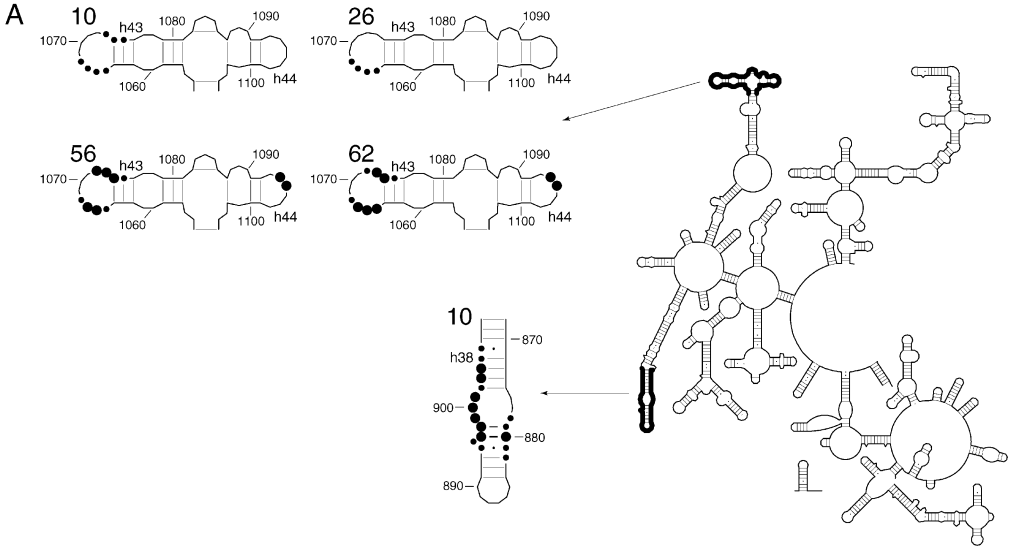
A
10
h43
1080
1090
1070
1060
1100
h44
26
56
62
10
h38
870
900
880
890

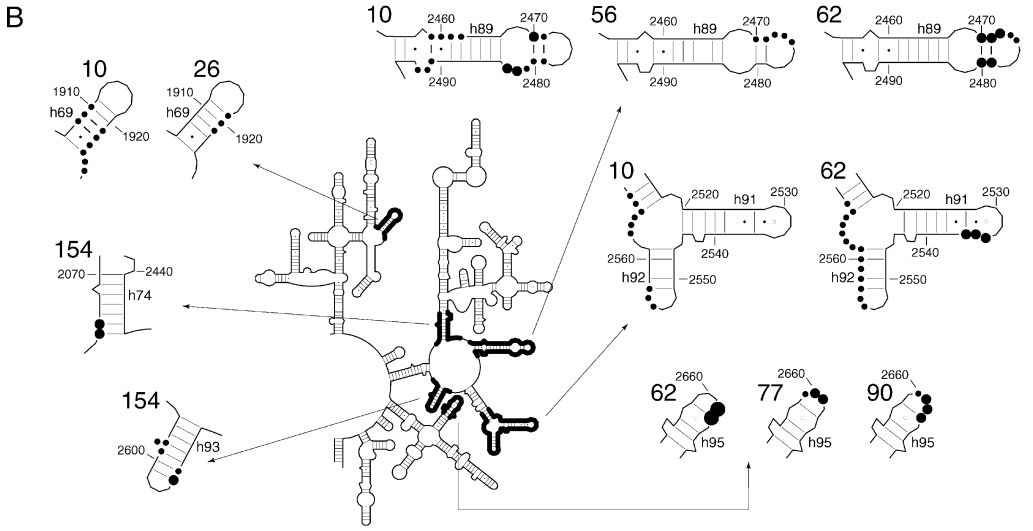
B
10
2460
h89
2470
2490
2480
56
62
10
1910
h69
1920
26
154
2070
2440
h74
2600
h93
2520
h91
2530
2540
2560
h92
2550
62
2660
h95
77
90

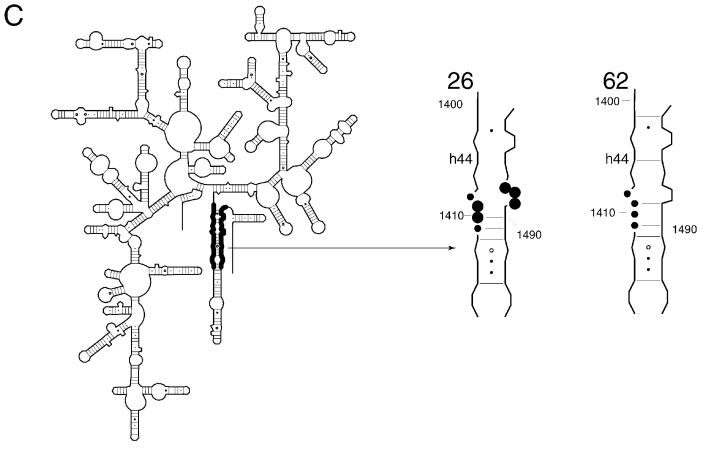
C
26
1400
h44
1410
1490
62

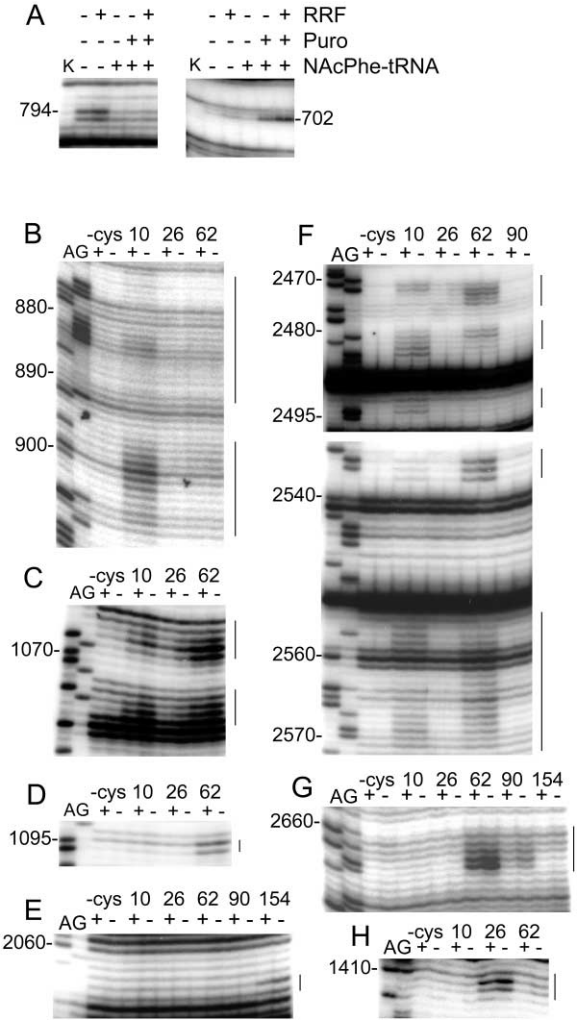

Figure 4. Directed Hydroxyl Radical Probing of 16S and 23S rRNA from Fe(II)-RRF-70S Ribosome-poly(U)-tRNA^{Phe} Complexes

(A) Chemical footprinting of 16S rRNA by tRNA in RRF-tRNA-mRNA-70S ribosome complexes. Complexes were probed with dimethyl sulfate and the RNA analyzed by primer extension. Complexes contained 70S ribosomes, poly(U) mRNA, and, where indicated, N-Acetyl-Phe-tRNA, RRF, or N-Acetyl-Phe-tRNA subjected to reaction with puromycin. Lane K, RNA from unmodified ribosomes.

(B–H) Hydroxyl radical cleavages of rRNA in 70S ribosome-mRNA complexes carried out as for Figure 2, in the presence (+) or absence (−) of tRNA. A and G are sequencing lanes. All other lanes are from ribosomes bound with mock-derivatized RRF(-cys) or with Fe-(II)-BABE-derivatized RRF, as indicated.

(B–G) 23S rRNA

(H) 16S rRNA

Directed probing from RRF in the 70S-mRNA-tRNA complexes gave results closely resembling those observed for the vacant 70S complex (Figures 4B–4H). In most cases, the observed cleavages for the two kinds of complexes were indistinguishable both in pattern and intensity, within experimental error, and no additional cleavages were observed. However, decreases in intensity were observed for some of the directed cleavages. Weaker cleavage was found for 23S rRNA in the L11 region from RRF positions 10 and 26 and in the sarcin loop from positions 62 and 90 (Figures 4C and 4G). Decreased cleavage intensity was also observed at the top of the penultimate stem in 16S rRNA from position 62 (Figure 4H). The close similarity in the cleavage patterns in the presence or absence of tRNA indicates that the overall position and orientation of RRF do not differ significantly. The observed decreases in intensity are most likely explained by localized structural changes in RRF and/or the ribosome, as discussed below.

Modeling the RRF-70S Ribosome Interaction

We used the probing data as constraints to model the position and orientation of RRF in the 5.5 Å crystal structure of the 70S ribosome-tRNA-mRNA complex (Yusupov et al., 2001). Strong, medium, and weak cleavage intensities constrained the α carbon of the Fe(II)-derivatized probing position to within 25 Å, 35 Å, or 50 Å, respectively, of the rRNA target (see Experimental Procedures). For each rRNA nucleotide cleaved from a given RRF probe, we generated a sphere centered on the position of the target nucleotide in the 70S ribosome crystal structure with a radius equal to the range corresponding to its cleavage intensity (Joseph et al., 1997). The allowed location of a given probe was thus constrained to the cloud of overlapping spatial volume common to all the rRNA spheres generated from that probe position (Figure 5A).

Among the four RRF structures, our probing constraints are satisfied by those of *E. coli, Thermus thermophilus*, and *Aquifex aeolicus*, although the data from the vacant 70S ribosome complex are best satisfied by the *E. coli* structure, which is shown in the accompanying figures. It was possible to accommodate all but probing position 77 of the *Thermotoga maritima* RRF structure to the constraints, due to the different rotational angle of its domain II around the axis of domain I. Essentially the same orientation was found for RRF using the probing data obtained from the vacant 70S or 70S-mRNA-tRNA complexes.

RRF is clearly located at the ribosome interface, with domain I roughly aligned horizontally across the front of the 50S subunit and domain II positioned between the sarcin loop, L11, and S12 (Figures 5B and 6). The general orientation of RRF is constrained by cleavage in the peptidyl transferase region from position 154, near the tip of domain I, and of the sarcin loop and L11 binding region from position 62 near the hinge end of domain II (Figure 7A). The orientation of domain II is

Figure 3. Location of Hydroxyl Radical Cleavages in 16S and 23S rRNA from Fe(II)-RRF-70S Ribosome Complexes

Cleavage strengths are scored as strong (large circles), medium (medium circles), or weak (small circles) as described in Experimental Procedures.

(A) Cleavages in the 5′ half of 23S rRNA from RRF positions 10, 26, 56, and 62.

(B) Cleavages in the 3′ half of 23S rRNA from RRF positions 10, 26, 56, 62, 77, 90, and 154.

(C) Cleavages in 16S rRNA from RRF positions 26 and 62.

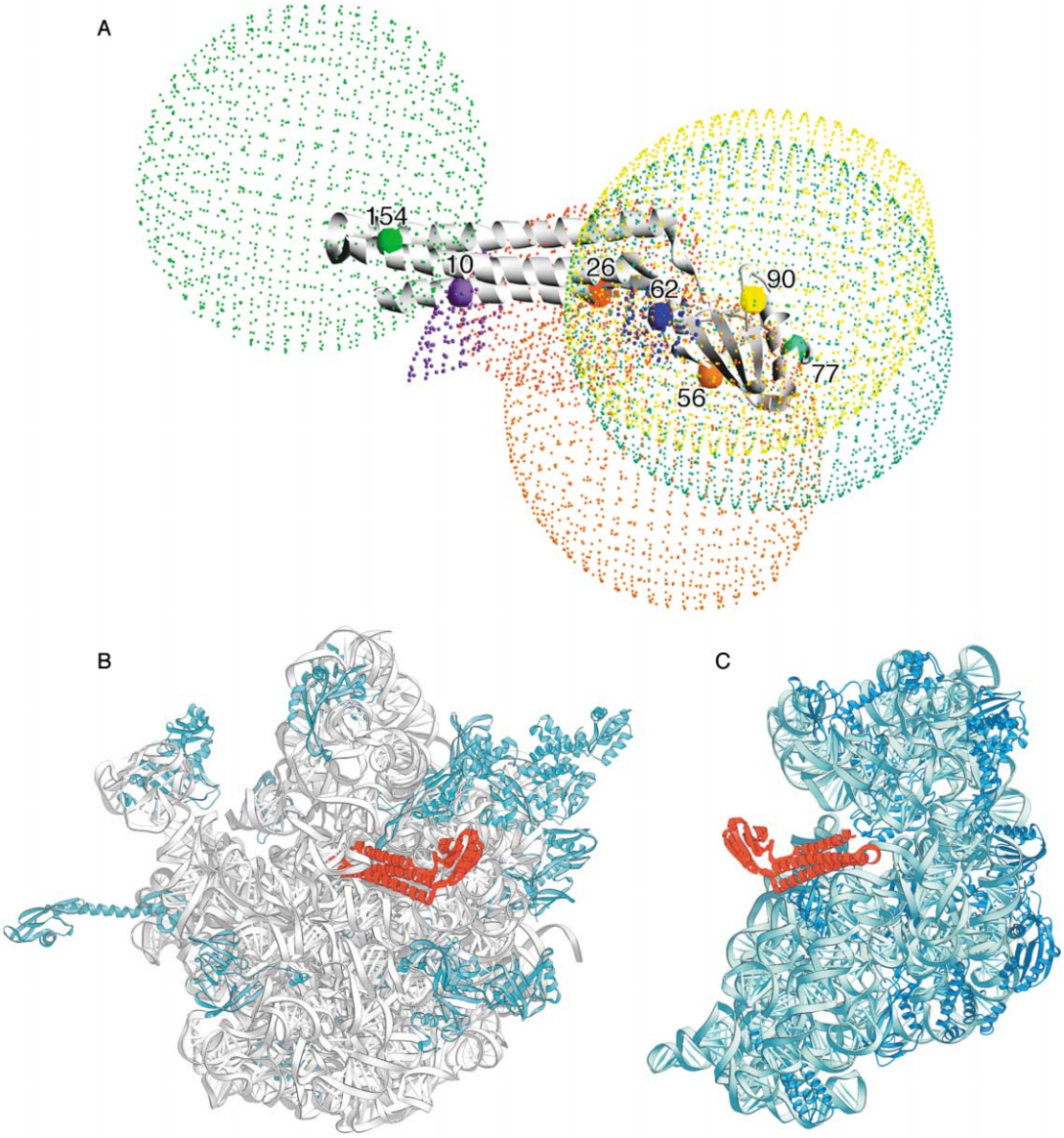

Figure 5. Positioning RRF in the 70S Ribosome

(A) Calculated clouds generated for the allowed positions of each RRF probing position. The *E. coli* RRF crystal structure (Kim et al., 2000) is shown in this and the following figures (light gray). The cloud of overlapping spatial volume is shown for each RRF probing position, based on the positions of cleavage targets in rRNA (see text): 10 (purple), 26 (red), 56 (orange), 62 (blue), 77 (turquoise), 90 (yellow), and 154 (green). (B and C) Modeled position and orientation of RRF (red) relative to the 50S and 30S subunits, respectively, in the 70S ribosome crystal structure (Yusupov et al., 2001).

(B) Crown view of the 50S subunit; 23S rRNA shown in light gray, proteins in light blue.

(C) View of the 30S subunit, rotated 180° from (B); 16S rRNA in light green, proteins in blue.

additionally constrained by cleavage of the L11 binding region from position 56, on the upper face of domain II, and of the sarcin loop from positions 90 and 77, on the opposite face of domain II (Figure 7B). The orientation of domain I is further constrained by cleavage at the top of the penultimate stem of 16S rRNA from position 26, near the hinge, and cleavage of numerous elements of 23S rRNA that surround the A-tRNA binding region from position 10 (Figures 7C and 7D).

The modeled position of RRF on the 70S ribosome is strongly constrained; intersecting clouds were generated from the nucleotide cleavage data from each probing position and the RRF structure could be placed such that every probing position fit into its respective cloud (Figure 5A). The only set of target nucleotides that was not well-behaved were the cleavages in 23S rRNA helix 38 (the A site finger). Since the A site finger is a known mobile element (Ban et al., 2000; Frank and Agrawal, 2000; Harms et al., 2001; Yusupov et al., 2001), we calculated clouds for position 10 with and without the data from helix 38. When the helix 38 data were included, no intersecting cloud was obtained for the location of position 10, but when the helix 38 data were omitted, the resulting intersecting volume constrained position

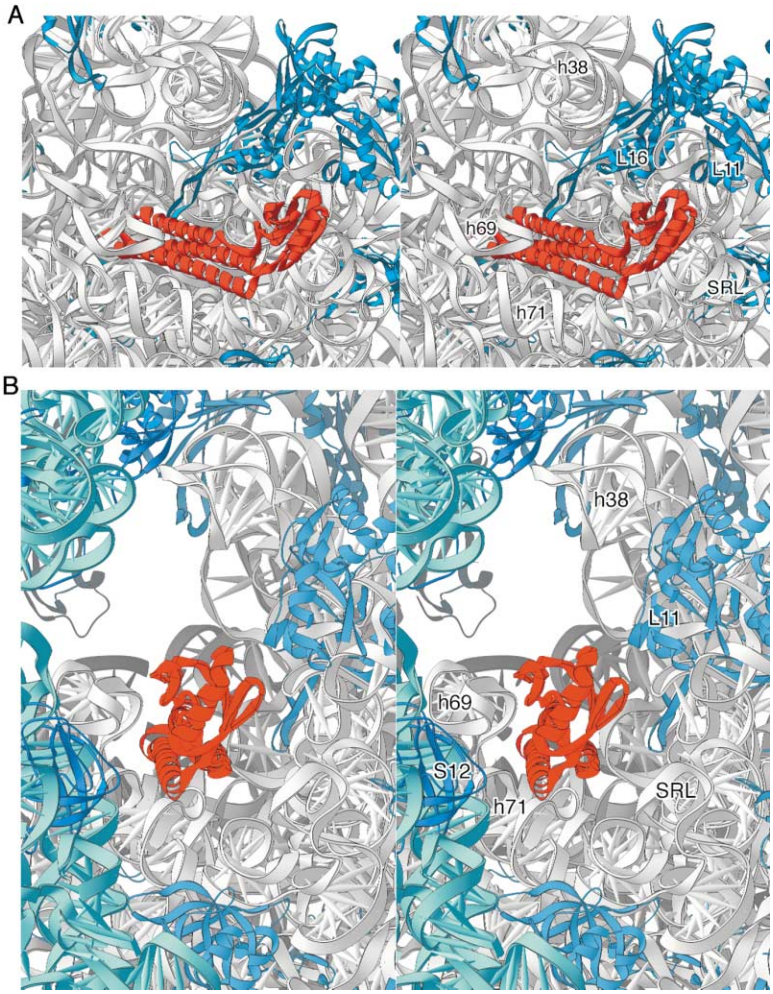

Figure 6. Stereo Views of the Modeled Position of RRF in the 70S Ribosome

(A) Close-up crown view of the 50S subunit: 23S rRNA (light gray), 50S proteins L11 and L16 (blue), *E. coli* RRF (red).

(B) Ribosome interface from L11 side: 23S rRNA (light gray), 16S rRNA (light green), 50S protein L11 and 30S protein S12 (blue), RRF (red).

10 to a location that was consistent within the context of clouds generated from each of the other six probing positions (Figure 5A). This suggests that the A site finger may have a different orientation in the 70S ribosome-RRF complexes than in the reference 70S ribosome crystal structure.

According to our modeling, domain I of RRF lies in a cleft formed by the parallel helices 69 and 71 in the middle of the lateral arm of the 50S subunit interface (Figures 5B and 6). RRF most closely approaches nucleotides 1942-1947 and 1963-1965 of helix 71 and 1907-1908 of helix 69 at its universally conserved residues R129 and R132 (mutations which confer lethal phenotypes; Janosi et al., 2000), E122, and the highly conserved N130, R133, K144, and Q161, all located in domain I. These residues are thus candidates for potential contact regions between RRF and the ribosome.

Discussion

The RRF protein structure has been shown to closely resemble that of tRNA (Selmer et al., 1999; Kim et al., 2000; Toyoda et al., 2000; Yoshida et al., 2001). This striking structural similarity has led to the hypothesis that RRF binds to the ribosomal A site of the posttermination complex in a tRNA-like orientation, such that domain I would point toward the decoding site of the 30S subunit and domain II toward the peptidyl transferase site of the 50S subunit (Selmer et al., 1999). According to this model, RRF would then be translocated to the P site by EF-G, resulting in disassembly of the complex into free ribosome, mRNA, and tRNA. Surprisingly, our probing data clearly constrain RRF in an orientation that is unlike that of any of the crystallographically observed tRNA binding positions, or any that have been observed by cryo-EM reconstruction (Agrawal et al., 1996). For example, a probe at position 154, the region of RRF proposed to correspond to the tRNA anticodon loop, cleaves 23S rRNA around the peptidyl transferase center of the 50S subunit, whereas probes in the region of RRF previously assigned to the acceptor arm of tRNA cleave the sarcin loop (Figures 7A and 7B). A detailed fitting of the factor based on the complete set of constraints leads to an orientation that is nearly orthogonal to those of the A- and P-tRNAs (Figure 8A).

This finding suggests that apparent structural mimicry of RNA by proteins, such as has been observed for elongation factor EF-G, the translational release factors, and RRF (for review, see Nakamura et al., 2000; Nissen et al., 2000; Ramakrishnan, 2002), does not always correspond to functional mimicry. In some cases, the tRNA-

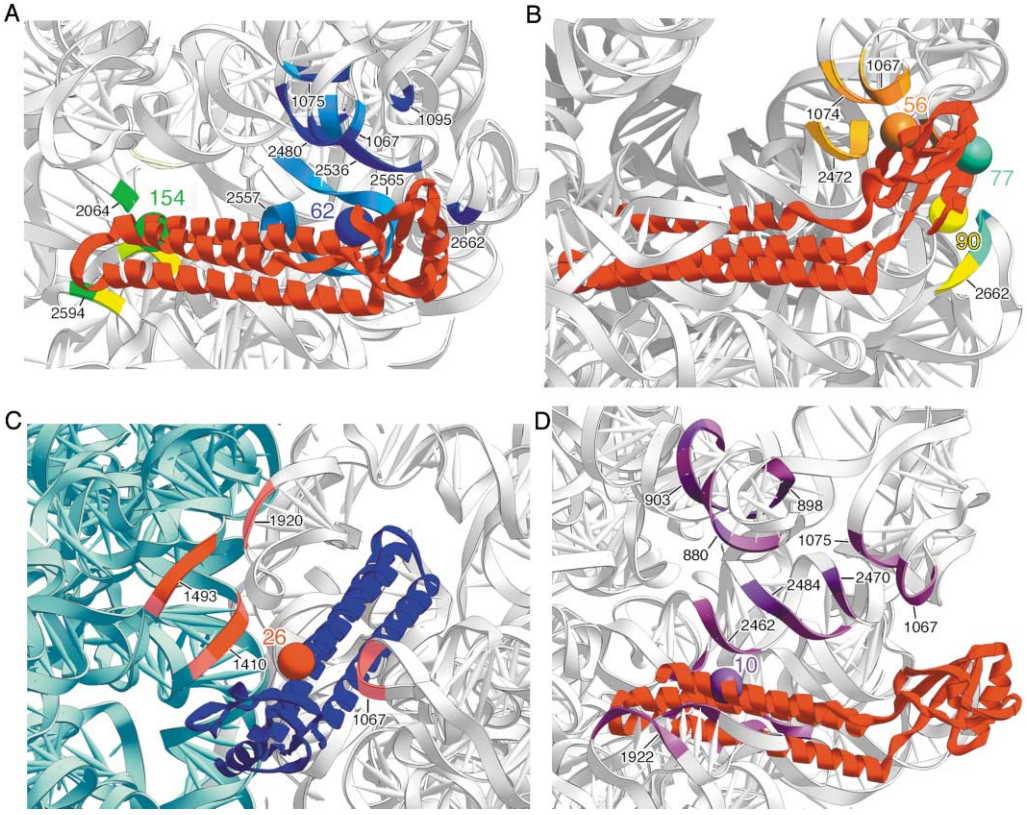

Figure 7. Proximities of rRNA Target Locations in the 70S Ribosome to Probing Positions on RRF

The ribosomal proteins are not shown. Nucleotide positions in rRNA are indicated using the *E. coli* numbering system. 23S and 16S rRNA cleaved from Fe(II) tethered to different positions on RRF are colored according to their respective probe positions.

(A) Cleavage of 23S rRNA from positions 62 (blue), and 154 (green) of RRF.

(B) Cleavage of 23S rRNA from RRF positions 56 (orange), 77 (turquoise), and 90 (yellow).

(C) Cleavage of 16S and 23S rRNA from position 26 (red) of RRF.

(D) Cleavage of 23S rRNA from position 10 (purple) of RRF. Strong and medium cleavages are shown in dark colors, weak cleavages in light colors.

like dimensions of certain translational factors may be dictated by the spatial constraints of the ribosomal intersubunit cavity, whose dimensions are closely tailored to the thickness of tRNA. For example, the triple-helix domains of RRF and RF2 and the α/β domain 4 of EF-G all have about the maximum thickness that can be accommodated in a cleft that is designed to fit an RNA double helix. Protein domains whose evolution is constrained in this way would have a tendency to resemble structural elements of tRNA.

Our model predicts that RRF interacts primarily with the 50S subunit, a prediction that is confirmed by our binding studies (Table 1), by earlier experiments that report a preferential interaction of matrix-immobilized

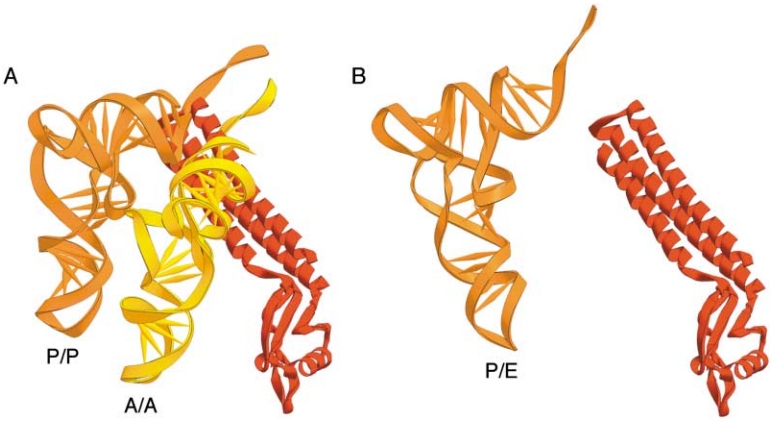

Figure 8. Modeled Position of RRF Relative to the Positions of tRNA in the 70S Ribosome

E. coli RRF is shown in red.

(A) Classically bound A-tRNA (yellow) and P-tRNA (orange) as seen in the 70S-tRNA-mRNA cocrystal structure (Yusupov et al., 2001).

(B) Hybrid state P/E-tRNA, modeled by interpolation of the crystallographically determined positions of P- and E-tRNA's (Yusupov et al., 2001), based on chemical footprinting evidence (Noller et al., 2002).

RRF with 50S subunits over 30S subunits (Ishino et al., 2000) and by Hirokawa et al. (2002b). RRF overlaps with the 50S subunit A-tRNA binding site, in agreement with the finding that RRF competes for binding to ribosomes with release factor RF1 (Pavlov et al., 1997), which is believed to occupy the ribosomal A site, and also with deacylated tRNA (Hirokawa et al., 2002a). This placement is also consistent with the fact that the substrate for RRF, the posttermination complex, contains a vacant A site. Finally, RRF domain II is very close to the sarcin loop and L11 regions of 23S rRNA. Both of these features interact with EF-G (Hausner et al., 1987; Moazed et al., 1988; Agrawal et al., 1998), which, in addition to RRF, is required for posttermination complex disassembly (Hirashima and Kaji, 1972, 1973).

Interestingly, the main differences in rRNA cleavages from Fe(II)-RRF that we observed between the vacant 70S and 70S-mRNA-tRNA complexes were localized to the L11 and sarcin loop regions. The decreased intensities cannot be explained by protection by the bound P/E tRNA, since it is located at the opposite side of the ribosome from the L11 and sarcin regions (Yusupov et al., 2001; Noller et al., 2001, 2002). More likely, the differences are due to a localized structural change in RRF and/or in the L11-sarcin region of the 50S subunit. Movement of the flexible domain II of RRF to an orientation that more closely resembles that of the *T. thermophilus*, *T. maritima*, or *A. aeolicus* structures would explain the decreased cleavage intensities for the sarcin loop from position 90 in domain II; the more modest changes in intensity observed for position 62 are consistent with its location close to the hinge connecting domains I and II. It is unlikely that the decreased cleavage of the L11 region from positions 10 and 26 is caused by movement of domain I, since there are no observable differences in intensity for any of the other numerous cleavages from position 10. However, the aforementioned movement of domain II could shield the L11 RNA from attack by radicals generated from positions 10 and 26 in domain I. Alternatively, the orientation of the L11 and sarcin regions of the 50S subunit could be shifted in the tRNA-containing complex.

In our model, RRF clashes with the positions of the acceptor arms of the A- and P-tRNAs in the 70S ribosome crystal structure (Figure 8A). However, the functional substrate for RRF is a 70S ribosome containing a vacant A site and a peptidyl-tRNA that must be subjected to prior deacylation by RF1, RF2, or puromycin in order for RRF to function (Hirashima and Kaji, 1970; Ogawa and Kaji, 1975; Karimi et al., 1999). Deacylation of peptidyl-tRNA by reaction with puromycin results in a P/E hybrid binding state (Moazed and Noller, 1989a; Noller et al., 2002) in which the acceptor end of the tRNA moves into the 50S subunit E site, thus avoiding a clash with our positioning of RRF (Figure 8B). We would predict that deacylation of peptidyl-tRNA by RF1 or RF2 will lead to the same result. Our probing experiments show that the position of RRF in ribosome complexes containing mRNA and deacylated tRNA in the P/E state is essentially similar to that observed in vacant 70S ribosome complexes.

It is not well understood how RRF, in concert with EF-G and GTP, disassembles the posttermination complex to recycle ribosomes for additional rounds of translation. Our model suggests that domain I of RRF binds the ribosome near helices 69 and 71 of 23S rRNA and positions domain II near the L11 region and sarcin loop, where it may interact with EF-G. Helices 69 and 71 both make interface contacts with helix 44 of 16S rRNA, the penultimate stem, which in turn makes important contacts with the mRNA around the neck of the 30S subunit (Yusupova et al., 2001). The surface of 16S rRNA that contacts helix 69 also forms the binding site for the C domain of initiation factor IF3 (Moazed et al., 1995; Dallas and Noller, 2001). A possible mechanism for disassembly is that EF-G acts through RRF on helices 69 and 71 of 23S rRNA, resulting in distortion of the penultimate stem to cause loss of mRNA and the deacylated tRNA from the ribosome. Alternatively, or in addition, movement of helix 69 may open up the IF-3 binding site on the 30S subunit, allowing IF-3 to promote complete dissociation of the ribosomal subunits and removal of the deacylated tRNA from the 30S subunit.

Finally, our findings do not exclude the possibility that RRF, like tRNA, can bind to the ribosome at different sites during different functional states. Further studies of this type, using complexes of RRF bound in the presence of EF-G, may be able to address this question and shed light on the possible role of interdomain movement of RRF in ribosome disassembly.

Experimental Procedures

Materials

Tight-couple 70S ribosomes were prepared from *E. coli* MRE600 as described (Powers and Noller, 1991) with the following modifications. The cleared cell lysate was layered on two 10 ml 1.1 M sucrose cushions in 20 mM Tris-HCl (pH 7.5), 500 mM NH_4Cl, 10.5 mM $MgCl_2$, 0.5 mM EDTA, 6 mM βME in 26 ml polycarbonate bottles and ultracentrifuged for 20.5 hr at 38,000 rpm in a Beckman Ti60 rotor. The resulting ribosome pellet was resuspended in 2 ml of 20 mM Tris-HCl (pH 7.5), 100 mM NH_4Cl, 10.5 mM $MgCl_2$, 0.5 mM EDTA, 6 mM βME; the NH_4Cl concentration was increased to 0.5 M; and the volume was increased to 26 ml. The ribosomes were then pelleted and further purified as described (Powers and Noller, 1991).

Construction of RRF Mutants

The RRF(-cys) mutant was generated from the *E. coli* wild-type RRF gene construct pRR2 (Shimizu and Kaji, 1991) by the QuikChange site-directed mutagenesis method (Stratagene) using primers 5′-TAC GCATGGACAAATCCGTAGAAGCGTCAA and 5′-TTGAACGCTTC TACGGATTTGTCCATGCGTA. The resulting RRF(C16S) gene construct was sequenced and then cloned into pET21b (Novagen) by PCR amplification of the gene with primer 5′-TTTCCATCCCATAT GATTAGCGATATCAGAAAAGATGCTGAA, which adds an *Nde* I restriction site to the 5′ end and changes the RRF start codon to AUG, and primer 5′-TATGGATCCTCAGAACTGCATCAGTTCTGCTTCTTT GTC, which adds a *Bam*H I restriction site the 3′ end. The PCR-amplified product was digested with *Nde* I and *Bam*H I and ligated into identically digested pET21b. Cysteine codons were introduced into the RRF(-cys) gene construct by site-directed mutagenesis (Kunkel, 1985) at positions 10, 26, 56, 62, 77, 90, 119, 137, 154, and 169. The mutations were confirmed by sequencing.

Functional Activity of RRF(C16S)

The pRR2 plasmid containing the RRF(-cys) gene was transformed into temperature-sensitive RRF strain LJ14 (Janosi et al., 1998) and tested for its ability to rescue the strain. To control for possible recombination, a strain that has no functional RRF on the chromosome, LJ2708 (Rolland et al., 1999), and survives with a copy of functional RRF on a kanamycin-resistant plasmid was transformed with the ampicillin-resistant RRF(-cys) plasmid. The transformant was grown on just ampicillin media until the kanamycin plasmid

was lost, showing that the RRF(-cys) mutant alone was able to support growth of the strain.

Expression and Purification of RRF

Each mutant RRF protein was expressed in *E. coli* BLR(DE3) by growth at 37°C in LB plus ampicillin (100 μg/ml) to an A_{550} of 0.6–0.8, followed by induction with IPTG (1 mM final concentration) followed by growth for 3 hr. Cells were pelleted and resuspended in 20 mM Tris-HCl (pH 7), 10 mM KCl, and 6 mM βME, lysed by sonication, then centrifuged at 7000 rpm for 15 min in a JA20 rotor. The cysteine-free RRF protein and RRF mutated at positions 56, 62, 90, 119, 137, and 169 were soluble, whereas RRF proteins mutated at positions 10, 26, 77, and 154 formed inclusion bodies. In order to treat them all identically, we either dialyzed or resuspended each in S buffer A: 20 mM NaOAc (pH 5.6), 10 mM KCl, 6 M urea, and 6 mM βME. Proteins were then purified by FPLC chromatography at 4°C using a Resource S cation-exchange column (Pharmacia) and eluted with a 48 ml salt gradient from 10 mM to 210 mM KCl in S buffer A, in which all mutant RRF proteins eluted at ~40 mM KCl. The fractions containing RRF were dialyzed into Q-buffer A (20 mM Tris-HCL [pH 7.8], 10 mM KCl, 6 mM βME) and further purified by FPLC over a Resource Q anion-exchange column (Pharmacia), for which all of the mutant RRF proteins appeared in the flow-through. The flow-through fractions containing RRF were dialyzed into RRF storage buffer (10 mM Tris-HCL [pH 7.5], 50 mM NH_4Cl, 10 mM $MgCl_2$, and 3 mM βME), aliquoted, quick-frozen in liquid N_2, and stored at −80°C.

Derivatization of RRF Proteins

Derivatization of cysteine-containing RRF mutants and mock derivatization of RRF(-cys) was done essentially as described (Heilek et al., 1995). Fe(II)-BABE (100 nmol) or 140 nmol iodo-[^{14}C]-acetamide (Amersham, 59 mCi/mmol) was incubated with RRF (3.5 nmol) in 200 μl of RRF modification buffer (80 mM K-HEPES [pH 7.6], 50 mM NH_4Cl, 5 mM $MgCl_2$) at 37°C for 30 min (Fe(II)-BABE) or 15 min (iodo-[^{14}C]-acetamide), then stored on ice. Excess reagent was removed by ultrafiltration in Microcon 10 concentrators (Amicon) at 4°C at 9000 rpm, followed by four 300 μl washes with RRF storage buffer. Mock derivatization with cysteine-free RRF was included as a control. The extent of Fe(II)-BABE modification for each mutant was monitored by reactivity with a thiol-specific fluorescent coumarin reagent DCIA (Molecular Probes) as described (Lancaster et al., 2000) and estimated to be 80%–90%. The extent of modification with iodo-[^{14}C]-acetamide was estimated by determining the amount of [^{14}C] by scintillation counting (120 cpm/pmol) and dividing this number by the protein concentration as determined by the Bradford method. Modification was found to be between 20% and 50%.

Binding Assay

[^{14}C]-acetamido-RRF mutant proteins (10 μM) were incubated alone (as a control) or with 70S ribosomes, 30S subunits, or 50S subunits (each at 1 μM) in RRF binding buffer (80 mM K-HEPES [pH 7.6], 25 mM KCl, 10 mM $MgCl_2$) at 37°C for 10 min, then on ice for 5 min. Unbound RRF protein was removed by filtration through Microcon 100 concentrators (Amicon) at 4°C and 3000 rpm, followed by three washes with RRF binding buffer. The [^{14}C]-RRF protein retained was scintillation-counted and its amount determined by subtracting the background counts from the control reaction lacking ribosomes and dividing by the estimated extent of modification for each mutant (see above).

Monosome to Polysome Conversion Assay

Reactions containing 0.6 A_{260} units of polysomes, 0.36 mM GTP, 15 pmol EF-G, 15 pmol RRF, and 50 μM puromycin in 9.1 mM Tris-HCl (pH 7.4), 7.3 mM NH_4Cl, 7.3 mM $Mg(OAc)_2$, 0.1 mM DTT in a final volume of 275 μl were incubated at 35°C for 10 min, then on ice for 2 min. The reactions were layered onto a 4.1 ml 10%–30% sucrose gradient in 10 mM Tris-HCl (pH 7.4), 10 mM $Mg(OAc)_2$, 50 mM NH_4Cl, 0.5 mM DTT and centrifuged for 75 min at 40,000 rpm in an SW 50.1 rotor. The gradients were fractionated, and the A_{254} of peak areas of monosomes and polysomes were measured. The peak area of the monosomes was divided by the peak area of both the monosomes and polysomes to calculate a percent conversion for each Fe(II)-RRF mutant protein and wild-type RRF. Background (in the absence of RRF) was subtracted from each value. Conversion by wild-type RRF was defined as 100% activity.

Construction of mRNA-tRNA-70S Complexes

E. coli $tRNA^{Phe}$ (Sigma) was charged with [^{14}C]phenylalanine (505 mCi/mmol), converted to N-actetyl-Phe-tRNA by reaction with acetic anhydride as described (Moazed and Noller, 1989b), and purified by FPLC chromatography on BD-cellulose (Robertson and Wintermeyer, 1981) to 1600 pmol/A_{260} unit. Complexes were formed by incubation of *E. coli* 70S ribosomes (1 μM) with poly(U) (20 A_{260} units/ml), and N-acetyl-[^{14}C]-Phe-tRNA (1.1 μM) at 37°C for 20 min in 80 mM K-HEPES (pH 7.6), 100 mM NH_4Cl, 10 mM $MgCl_2$, and 1 mM DTT. The complex was then reacted with puromycin (2 mM) for 20 min at 25°C, and the N-acetyl-[^{14}C]-Phe-puromycin product measured after extraction with ethylacetate (Robertson and Wintermeyer, 1981). Binding of N-acetyl-Phe-tRNA to the ribosome was assayed by filter binding, and binding of the N-acetyl-Phe-tRNA and deacylated tRNA in the P/P and P/E states, respectively, was confirmed by base-specific chemical probing, as described (Moazed and Noller, 1989a).

Directed Hydroxyl Radical Probing

Complexes containing either mock-derivatized RRF(-cys) (10 μM) or Fe(II)-RRF (10 μM) bound to vacant 70S ribosomes (1 μM) were formed by incubation in RRF binding buffer (see above) at 37°C for 10 min, then on ice for 5 min. Free Fe(II)-RRF was removed by filtration through Microcon 100 concentrators, as described above. Complexes containing ribosomes, mRNA, and with or without N-acetyl-Phe-tRNA were formed and treated with puromycin as above, followed by the addition of a 10-fold molar excess of either mock-derivatized RRF(-cys) or Fe(II)-RRF over ribosomes, and incubation at 37°C for 10 min, then on ice for 5 min. Probing of all RRF-containing complexes were done as described (Heilek et al., 1995). Briefly, 1 μl of 250 mM ascorbic acid and 1 μl of 2.5% hydrogen peroxide were added to 50 μl of the Fe(II)-RRF-70S ribosome complex and incubated on ice for 10 min. The reaction was stopped by adding 2.5 μl of 80 mM thiourea. The rRNA was precipitated with 0.3 M NaOAc and 2.5 volumes of 95% ethanol, resuspended in 0.3 M NaOAc, 10% SDS, and 5 mM EDTA, and extracted three times with phenol and twice with chloroform. The rRNA was reprecipitated, resuspended in 100 μl of ddH_2O, and stored at −20°C. The precise location of 16S and 23S rRNA backbone cleavage was detected by primer extension with reverse transcriptase (Stern et al., 1988). Cleavage intensities were scored visually, according to whether the primer extension stops were strong (at least twice as strong as adjacent sequencing bands), weak (less than half as strong as adjacent sequencing bands), or medium (between strong and weak) (Joseph et al., 1997).

Modeling

RRF was modeled in the 5.5 Å 70S ribosome crystal structure (Yusupov et al., 2001) using the program O (Jones and Kjeldgaard, 1997). The coordinates from three crystal structures (Selmer et al., 1999; Kim et al., 2000; Toyoda et al., 2000) and one NMR structure (Yoshida et al., 2001) of RRF were used. The distance relation between rRNA cleavage intensity and target to probe distance was determined to be strong at 0–25 Å, medium at 0–35 Å, and weak at 0–50 Å. This relation was calibrated by measuring the crystallographically determined distances between the α carbon of probe positions on ribosomal proteins to the phosphate backbone of their rRNA targets from previous Fe-BABE probing studies. These distances were then compared with the observed rRNA cleavage intensities reported for each probe (Heilek et al., 1995; Heilek and Noller, 1996a, 1996b; Culver and Noller, 1998; Culver et al., 1999; Lancaster et al., 2000) and plotted (A. Dallas, L.L., and H.F.N, unpublished). The predicted maximum probe to target distances were similar to those previously obtained by an earlier calibration method (Joseph et al., 1997). However, our more recent calibration emphasizes the possible effects of quenching and RNA orientation, both of which can lead to diminished cleavage intensities. These effects are taken into account in the present range values. Structure figures were drawn using the program RIBBONS (Carson, 1997).

Acknowledgments

We thank B. Weiser for writing the clouds program, A. Baucom for help with the figures, K. Lieberman, K. Fredrick, and R. Hickerson for critical comments on the manuscript, and A. Dallas for unpublished results. This work was supported by NIH grants GM17129 and GM59140 (to H.F.N.) and GH60429 (to A.K.) and a grant from the W.M. Keck Foundation to the Center for Molecular Biology of RNA.

Received: April 29, 2002
Revised: August 7, 2002

References

Agrawal, R.K., Penczek, P., Grassucci, R.A., Li, Y., Leith, A., Nierhaus, K.H., and Frank, J.F. (1996). Direct visualization of A-, P-, and E-site transfer RNAs in the *Escherichia coli* ribosomes. Science *271*, 1000–1002.

Agrawal, R.K., Penczek, P., Grassucci, R.A., and Frank, J. (1998). Visualization of elongation factor G on the *Escherichia coli* 70S ribosome: the mechanism of translocation. Proc. Natl. Acad. Sci. USA *95*, 6134–6138.

Ban, N., Nissen, P., Hansen, J., Moore, P.B., and Steitz, T.A. (2000). The complete atomic structure of the large ribosomal subunit at 2.4 Å resolution. Science *289*, 905–920.

Carson, M. (1997). Ribbons. Methods Enzymol. *277B*, 493–505.

Culver, G.M., and Noller, H.F. (1998). Directed hydroxyl radical probing of 16S ribosomal RNA in ribosomes containing Fe(II) tethered to ribosomal protein S20. RNA *4*, 1471–1480.

Culver, G.M., Heilek, G.M., and Noller, H.F. (1999). Probing the rRNA environment of ribosomal protein S5 across the subunit interface and inside the 30S subunit using tethered Fe(II). J. Mol. Biol. *286*, 355–364.

Dallas, A., and Noller, H.F. (2001). Interaction of translation initiation factor 3 with the 30S ribosomal subunit. Mol. Cell *8*, 855–864.

Frank, J., and Agrawal, R.K. (2000). A ratchet-like inter-subunit reorganization of the ribosome during translocation. Nature *406*, 318–322.

Freistroffer, D.V., Pavlov, M.Y., MacDougall, J., Buckingham, R.H., and Ehrenberg, M. (1997). Release factor RF3 in *E. coli* accelerates the dissociation of release factors RF1 and RF2 from the ribosome in a GTP-dependent manner. EMBO J. *16*, 4126–4133.

Harms, J., Schluenzen, F., Zarivach, R., Bashan, A., Gat, S., Agmon, I., Bartels, H., Franceschi, F., and Yonath, A. (2001). High resolution structure of the large ribosomal subunit from a mesophilic eubacterium. Cell *107*, 679–688.

Hausner, T.P., Atmadja, J., and Nierhaus, K.H. (1987). Evidence that the G2661 region of 23S rRNA is located at the ribosomal binding sites of both elongation factors. Biochimie *69*, 911–923.

Heilek, G.M., and Noller, H.F. (1996a). Site-directed hydroxyl radical probing of the rRNA neighborhood of ribosomal protein S5. Science *272*, 1659–1662.

Heilek, G.M., and Noller, H.F. (1996b). Directed hydroxyl radical probing of the rRNA neighborhood of ribosomal protein S13 using tethered Fe(II). RNA *2*, 597–602.

Heilek, G.M., Marusak, R., Meares, C.F., and Noller, H.F. (1995). Directed hydroxyl radical probing of 16S rRNA using Fe(II) tethered to ribosomal protein S4. Proc. Natl. Acad. Sci. USA *92*, 1113–1116.

Hirashima, A., and Kaji, A. (1970). Factor dependent breakdown of polysomes. Biochem. Biophys. Res. Commun. *41*, 877–883.

Hirashima, A., and Kaji, A. (1972). Factor-dependent release of ribosomes from messenger RNA. Requirement for two heat-stable factors. J. Mol. Biol. *65*, 43–58.

Hirashima, A., and Kaji, A. (1973). Role of elongation factor G and a protein factor on the release of ribosomes from messenger ribonucleic acid. J. Biol. Chem. *248*, 7580–7587.

Hirokawa, G., Kiel, M.C., Muto, A., Kawai, G., Igarashi, K., Kaji, H., and Kaji, A. (2002a). Binding of ribosome recycling factor (RRF) to ribosomes—comparison with tRNA. J. Biol. Chem., in press. Published online July 22, 2002. 10.1074/jbc.M206295200.

Hirokawa, G., Kiel, M.C., Muto, A., Selmer, M., Raj, V.S., Liljas, A., Igarashi, K., Kaji, H., and Kaji, A. (2002b). Post-termination complex disassembly by ribosome recycling factor, a functional tRNA mimic. EMBO J. *21*, 2272–2281.

Inokuchi, Y., Hirashima, A., Sekine, Y., Janosi, L., and Kaji, A. (2000). Role of ribosome recycling factor (RRF) in translational coupling. EMBO J. *19*, 3788–3798.

Ishino, T., Atarashi, K., Uchiyama, S., Yamami, T., Saihara, Y., Yoshida, T., Hara, H., Yokose, K., Kobayashi, Y., and Nakamura, Y. (2000). Interaction of ribosome recycling factor and elongation factor EF-G with *E. coli* ribosomes studied by the surface plasmon resonance technique. Genes Cells *5*, 953–963.

Ito, K., Fujiwara, T., Toyoda, T., and Nakamura, Y. (2002). Elongation factor G participates in ribosome disassembly by interacting with ribosome recycling factor at their tRNA-mimicry domains. Mol. Cell *9*, 1263–1272.

Janosi, L., Shimizu, I., and Kaji, A. (1994). Ribosome recycling factor (ribosome releasing factor) is essential for bacterial growth. Proc. Natl. Acad. Sci. USA *91*, 4249–4253.

Janosi, L., Hara, H., Zhang, S., and Kaji, A. (1996a). Ribosome recycling by ribosome recycling factor (RRF)—an important but overlooked step of protein biosynthesis. Adv. Biophys. *32*, 121–201.

Janosi, L., Ricker, R., and Kaji, A. (1996b). Dual functions of ribosome recycling factor in protein biosynthesis: disassembling the termination complex and preventing translational errors. Biochimie *78*, 959–969.

Janosi, L., Mottagui-Tabar, S., Isaksson, L.A., Sekine, Y., Ohtsubo, E., Zhang, S., Goon, S., Nelken, S., Shuda, M., and Kaji, A. (1998). Evidence for in vivo ribosome recycling, the fourth step in protein biosynthesis. EMBO J. *17*, 1141–1151.

Janosi, L., Mori, H., Sekine, Y., Abragan, J., Janosi, R., Hirokawa, G., and Kaji, A. (2000). Mutations influencing the frr gene coding for ribosome recycling factor (RRF). J. Mol. Biol. *295*, 815–829.

Jones, T.A., and Kjeldgaard, M. (1997). Electron-density map interpretation. Methods Enzymol. *277B*, 173–208.

Joseph, S., Weiser, B., and Noller, H.F. (1997). Mapping the inside of the ribosome with an RNA helical ruler. Science *278*, 1093–1098.

Kaji, A., and Hirokawa, G. (2000). Disassembly of post termination complex by RRF (ribosome recycling factor), a possible new target for antimicrobial agents. In The Ribosome: Structure, Function, Antibiotics and Cellular Interactions, R.A. Garrett, S.R. Douthwaite, A. Liljas, A.T. Matheson, P.B. Moore, and H.F. Noller, eds. (Washington, DC: ASM Press), pp. 527–539.

Kaji, A., Kiel, M.C., Hirokawa, G., Muto, A., Inokuchi, Y., and Kaji, H. (2001). The fourth step of protein synthesis: disassembly of the post-termination complex is catalyzed by elongation factor G and ribosome recycling factor, RRF, a near perfect mimic of tRNA. Cold Spring Harb. Symp. Quant. Biol. *66*, 515–529.

Karimi, R., Pavlov, M.Y., Buckingham, R.H., and Ehrenberg, M. (1999). Novel roles for classical factors at the interface between translation termination and initiation. Mol. Cell *3*, 601–609.

Kim, K.K., Min, K., and Suh, S.W. (2000). Crystal structure of the ribosome recycling factor from *Escherichia coli*. EMBO J. *19*, 2362–2370.

Kunkel, T.A. (1985). Rapid and efficient site-specific mutagenesis without phenotypic selection. Proc. Natl. Acad. Sci. USA *82*, 488–492.

Lancaster, L., Culver, G.M., Yusupova, G.Z., Cate, J.H., Yusupov, M.M., and Noller, H.F. (2000). The location of protein S8 and surrounding elements of 16S rRNA in the 70S ribosome from combined use of directed hydroxyl radical probing and X-ray crystallography. RNA *6*, 717–729.

Moazed, D., and Noller, H.F. (1989a). Intermediate states in the movement of transfer RNA in the ribosome. Nature *342*, 142–148.

Moazed, D., and Noller, H.F. (1989b). Interaction of tRNA with 23S rRNA in the ribosomal A, P, and E sites. Cell *57*, 585–597.

Moazed, D., Robertson, J.M., and Noller, H.F. (1988). Interaction of

elongation factors EF-G and EF-Tu with a conserved loop in 23S RNA. Nature *334*, 362–364.

Moazed, D., Samaha, R.R., Gualerzi, C., and Noller, H.F. (1995). Specific protection of 16 S rRNA by translational initiation factors. J. Mol. Biol. *248*, 207–210.

Nakamura, Y., Ito, K., and Ehrenberg, M. (2000). Mimicry grasps reality in translation termination. Cell *101*, 349–352.

Nissen, P., Kjeldgaard, M., and Nyborg, J. (2000). Macromolecular mimicry. EMBO J. *19*, 489–495.

Noller, H.F., Yusopov, M.M., Yusupova, G.Z., Baucom, A., Lieberman, K., Lancaster, L., Dallas, A., Fredrick, K., Earnest, T.N., and Cate, J.H.D. (2001). Structure of the ribosome at 5.5 Å resolution and its interactions with functional ligands. Cold Spring Harb. Symp. Quant. Biol. *66*, 57–66.

Noller, H.F., Yusupov, M.M., Yusupova, G.Z., Baucom, A., and Cate, J.H. (2002). Translocation of tRNA during protein synthesis. FEBS Lett. *514*, 11–16.

Ogawa, K., and Kaji, A. (1975). Requirement for ribosome-releasing factor for the release of ribosomes at the termination codon. Eur. J. Biochem. *58*, 411–419.

Pavlov, M.Y., Freistroffer, D.V., Heurgue-Hamard, V., Buckingham, R.H., and Ehrenberg, M. (1997). Release factor RF3 abolishes competition between release factor RF1 and ribosome recycling factor (RRF) for a ribosome binding site. J. Mol. Biol. *273*, 389–401.

Poole, E., and Tate, W. (2000). Release factors and their role as decoding proteins: specificity and fidelity for termination of protein synthesis. Biochim. Biophys. Acta *1493*, 1–11.

Powers, T., and Noller, H.F. (1991). A functional pseudoknot in 16S ribosomal RNA. EMBO J. *10*, 2203–2214.

Ramakrishnan, V. (2002). Ribosome structure and the mechanism of translation. Cell *108*, 557–572.

Rao, A.R., and Varshney, U. (2001). Specific interaction between the ribosome recycling factor and the elongation factor G from *Mycobacterium tuberculosis* mediates peptidyl-tRNA release and ribosome recycling in *Escherichia coli*. EMBO J. *20*, 2977–2986.

Robertson, J.M., and Wintermeyer, W. (1981). Effect of translocation on topology and conformation of anticodon and D loops of tRNAPhe. J. Mol. Biol. *151*, 57–79.

Rolland, N., Janosi, L., Block, M.A., Shuda, M., Teyssier, E., Miege, C., Cheniclet, C., Carde, J.P., Kaji, A., and Joyard, J. (1999). Plant ribosome recycling factor homologue is a chloroplastic protein and is bactericidal in *Escherichia coli* carrying temperature-sensitive ribosome recycling factor. Proc. Natl. Acad. Sci. USA *96*, 5464–5469.

Ryoji, M., Berland, R., and Kaji, A. (1981). Reinitiation of translation from the triplet next to the amber termination codon in the absence of ribosome-releasing factor. Proc. Natl. Acad. Sci. USA *78*, 5973–5977.

Selmer, M., Al-Karadaghi, S., Hirokawa, G., Kaji, A., and Liljas, A. (1999). Crystal structure of *Thermotoga maritima* ribosome recycling factor: a tRNA mimic. Science *286*, 2349–2352.

Shimizu, I., and Kaji, A. (1991). Identification of the promoter region of the ribosome-releasing factor cistron (frr). J. Bacteriol. *173*, 5181–5187.

Stern, S., Moazed, D., and Noller, H.F. (1988). Structural analysis of RNA using chemical and enzymatic probing monitored by primer extension. Methods Enzymol. *164*, 481–489.

Toyoda, T., Tin, O.F., Ito, K., Fujiwara, T., Kumasaka, T., Yamamoto, M., Garber, M.B., and Nakamura, Y. (2000). Crystal structure combined with genetic analysis of the *Thermus thermophilus* ribosome recycling factor shows that a flexible hinge may act as a functional switch. RNA *6*, 1432–1444.

Yoshida, T., Uchiyama, S., Nakano, H., Kashimori, H., Kijima, H., Ohshima, T., Saihara, Y., Ishino, T., Shimahara, H., Yokose, K., et al. (2001). Solution structure of the ribosome recycling factor from *Aquifex aeolicus*. Biochemistry *40*, 2387–2396.

Yusupov, M., Yusupova, G., Baucom, A., Lieberman, K., Earnest, T.N., Cate, J.H., and Noller, H.F. (2001). Crystal structure of the ribosome at 5.5 Å resolution. Science *292*, 883–896.

Yusupova, G.Z., Yusupov, M., Cate, J.H.D., and Noller, H.F. (2001). The path of messenger RNA through the ribosome. Cell *106*, 233–241.